INTERNATIONAL JOURNAL FOR NUMERICAL METHODS IN FLUIDS
Int. J. Numer. Meth. Fluids 2007; **55**:785–791
Published online 5 April 2007 in Wiley InterScience (www.interscience.wiley.com). DOI: 10.1002/fld.1493

A simple axisymmetric extension to virtual cell embedding

J. Tang*, †

Department of Mechanical Engineering, The University of Queensland, Brisbane, Qld. 4072, Australia

SUMMARY

Virtual cell embedding (VCE) is a simple cartesian gridding method that subdivides cells into discrete subcells to obtain the approximate obstructed cell area and side lengths. It can be used to make a very fast calculation method for the Euler equations in two dimensions. However, the original procedure for two spatial dimensions is inadequate for axisymmetric geometries, where radial co-ordinates of cells and interfaces need to be known. Presented in this paper is a short, simple extension of the VCE method to handle axisymmetric cases with an accuracy consistent with the basic VCE surface representation in planar geometries. The method will be tested in basic conical flow simulations to show its usefulness for practical engineering design purposes. Copyright © 2007 John Wiley & Sons, Ltd.

Received 1 September 2006; Revised 18 February 2007; Accepted 21 February 2007

KEY WORDS: virtual cell embedding; VCE; cartesian grid; axisymmetric formulation; subcell; conical flow

1. BASIC VCE METHODOLOGY

A good description of the virtual cell embedding (VCE) method has been given by Landsberg *et al*. [1] and Landsberg and Boris [2] so a brief introduction to the basic VCE method in two spatial dimensions will be given here. First, as in Figure 1(a) the cell is subdivided into a lattice of discrete 'subcells'. Each subcell is tested if it is obstructed by a body. This way the approximate obstructed area and side lengths (or interfaces) can be determined.

The surface cutting through the cell is approximated as a single straight wall using the obstructed side lengths, as seen in the example in Figure 1(b). In this example, the *net obstructed* length along the x-axis l_x is found by $l_x = l_{x\mathrm{r}} - l_{x\mathrm{l}}$, and similarly for l_y. Then the average wall surface normal $\mathbf{n}_{\mathrm{avg}}$ is

$$\mathbf{n}_{\mathrm{avg}} = \sum_i \widehat{\mathbf{n}}_i l_i, \quad i = x, y \tag{1}$$

*Correspondence to: J. Tang, Department of Mechanical Engineering, The University of Queensland, Brisbane, Qld. 4072, Australia.
†E-mail: s363257@student.uq.edu.au

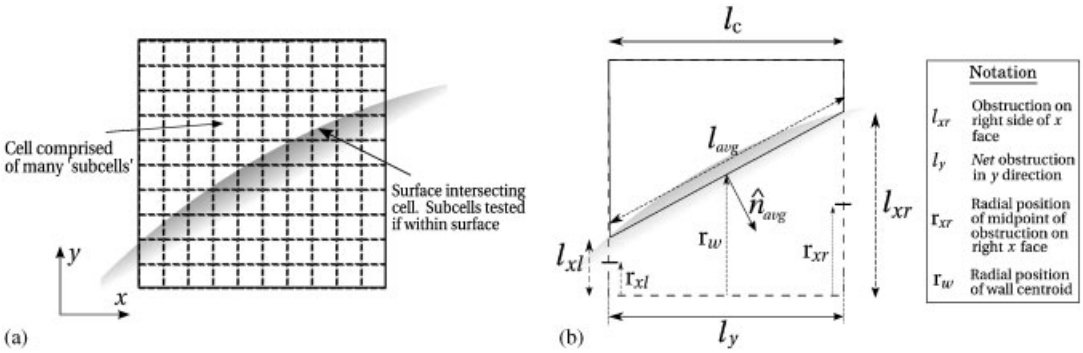

Figure 1. VCE methodology.

where $\hat{\mathbf{n}}_i$ is the unit vector along the axis i. The corresponding wall surface length l_{avg} is

$$l_{\text{avg}} = \|\mathbf{n}_{\text{avg}}\| \tag{2}$$

2. AXISYMMETRIC EXTENSION

The axisymmetric Euler equations in the integral form are

$$\frac{\partial}{\partial t}\int_A \mathbf{U}\,\mathrm{d}A + \int_l r\mathbf{F}\cdot\hat{\mathbf{n}}\,\mathrm{d}l = \int_V \mathbf{Q}\,\mathrm{d}A \tag{3}$$

$\mathbf{U}$ is the vector of conserved quantities $\mathbf{U} = [\rho, \rho u, \rho v, \rho E]^{\mathrm{T}}$, $\mathbf{F}$ the vector of fluxes, t the time dimension, ρ the density, u and v are velocity components in the x and y, directions, respectively, and E is the total energy per mass $E = e + \rho(u^2 + v^2)/2$, $\hat{\mathbf{n}}$ is the outward unit normal on the surface l which bounds the control volume A.

If the x-axis is the symmetry axis and y-axis the radial axis, then r is the radial co-ordinate at an interface and $\mathbf{Q} = [0, 0, p/r, 0]^{\mathrm{T}}$ where p is the pressure in the cell. Additionally A becomes the volume per radian. The cell-centred finite volume discretization of Equation (3) is given by

$$\frac{\mathrm{d}\mathbf{U}_{\mathrm{c}}}{\mathrm{d}t} = -\frac{1}{A_{\mathrm{c}}}\sum_{\mathrm{if}} r_{\mathrm{if}}\mathbf{F}_{\mathrm{if}}\cdot\hat{\mathbf{n}}_{\mathrm{if}}l_{\mathrm{if}} + \mathbf{Q} \tag{4}$$

where the subscript 'if' stands for interface, A_{c} is the cell volume, and $\mathbf{U}_{\mathrm{c}}$ is the cell-centred state vector. The volume per radian $A_{\mathrm{c}} = Ar_{\mathrm{c}}$, where A is the cell area and r_{c} the cell's average radial co-ordinate.

It can be seen that the base VCE scheme is only suitable for planar flow as the axisymmetric equations require additional information—the radial co-ordinates of the cell centre r_{c} and its fluid interfaces, i.e. the unobstructed side lengths r_{l} and wall surface r_{w}. How these quantities can be found is discussed below.

DOI: 10.1002/fld

2.1. Obtaining cell-centre and interface radial co-ordinates

The VCE subcell division can be used to calculate r_c (the cell's average radial co-ordinate) and r_l (the average radial co-ordinate of its unobstructed interfaces) if the radial co-ordinates of each subcell are stored and then averaged in the summation, i.e. $r_{c/l} = \sum_N r_{s_{c/l}}/N$, where r_s is the radial co-ordinate of a subcell, and N the total number of fluid subcells, i.e. unobstructed subcells.

2.2. Obtaining the wall radial co-ordinate

The wall radial co-ordinate r_w can be found by taking advantage of the fact that VCE always gives straight surface representations. With the help of Figure 1(b), first shift the origin to the lower left cell corner, and assume the cell is square of length l_c. In a similar manner to finding r_l now the average *obstructed* radial co-ordinates on the east and west faces r_{xr} and r_{xl}, respectively, are found. Now consider two cases: (1) when the surface normal is pointing downward or sideways (i.e. its radial co-ordinate is negative or zero respectively); and (2) when it is pointing upward.

1. *Downward or sideways surface normal*: With the help of Figure 2(a), note that r_{xr} and r_{xl} represent the midpoint of obstruction on a side, so that very simply $r_w = r_{xr} + r_{xl}$.
2. *Upward surface normal*: With the help of Figure 2(b), this case can also been seen as case (1) if the origin is shifted to the top right cell corner and the transformation $r' = l_c - r$ is applied. However, if either r_{xr} or r_{xl} are 0, then likewise r'_{xr} or r'_{xl}, respectively, are 0 (as a zero value means that no obstruction is present). Then $r'_w = r'_{xr} + r'_{xl}$, and finally transforming back, $r_w = l_c - r'_w$.

   Thus

$$r'_{x(l/r)} = \begin{cases} 0 & \text{when } r_{x(l/r)} = 0 \\ l_c - r_{x(l/r)} & \text{when } r_{x(l/r)} > 0 \end{cases}$$

   Then $r_w = l_c - (r'_{xr} + r'_{xl})$.

It should be noted from Figures 2(a) and (b) that it is equally possible to use the average unobstructed radial co-ordinates $\tilde{r}_{xr}$ and $\tilde{r}_{xl}$ instead of r_{xr} and r_{xl}.

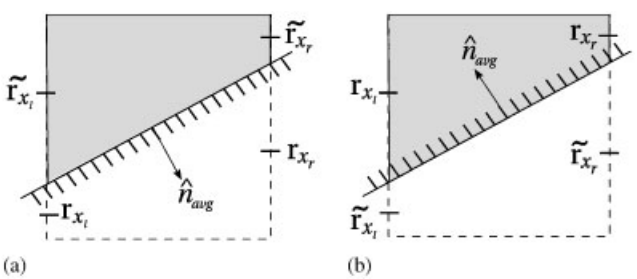

Figure 2. Two surface normal configurations: (a) downward surface normal and (b) upward surface normal.

DOI: 10.1002/fld

3. NUMERICAL RESULTS

Although Landsberg and Boris [2] has done a two-dimensional VCE accuracy study with an airfoil geometry and demonstrated that VCE can produce good results, here simple supersonic conical flow is investigated. This is also an important test case as: (i) VCE computes approximated surfaces that might be slightly oriented into or away from the flow—a numerical equivalent of 'surface roughening'; and (ii) conical flow solutions can be easily computed, e.g. using the method of Taylor and Maccoll [3], giving easy comparisons (in the steady-state limit, constant property lines are generators from the cone vertex).

In all the simulations below the half cone angle is 20° and a uniform cartesian grid is used with the area ratio of a cell to the triangle (representing the cone) being roughly 1.5×10^{-4}. The axisymmetric Euler equations (Equation (4)) were solved with an explicit two-stage Runge–Kutta method using the standard MUSCL technique [4] and a minmod limiter [5]. The flux solver used is the AUSMDV [6]. An ideal gas is used with ratio of specific heats $\gamma = 1.4$. As with most classical cartesian cell methods, cells with very small volume fractions (say below 10% of their basis areas) are merged with larger neighbouring cells to prevent excessively small timesteps.

3.1. Steady-state conical flow

The steady-state flow over the cone ($M_\infty = 2.5$) is considered here. This test case incorporates a subcell refinement study where the number of subcells (for both the area and side lengths) used are 32, 64, 128, and 256. Some density contours for the conical flow for various subcell resolutions can be seen in Figure 3.

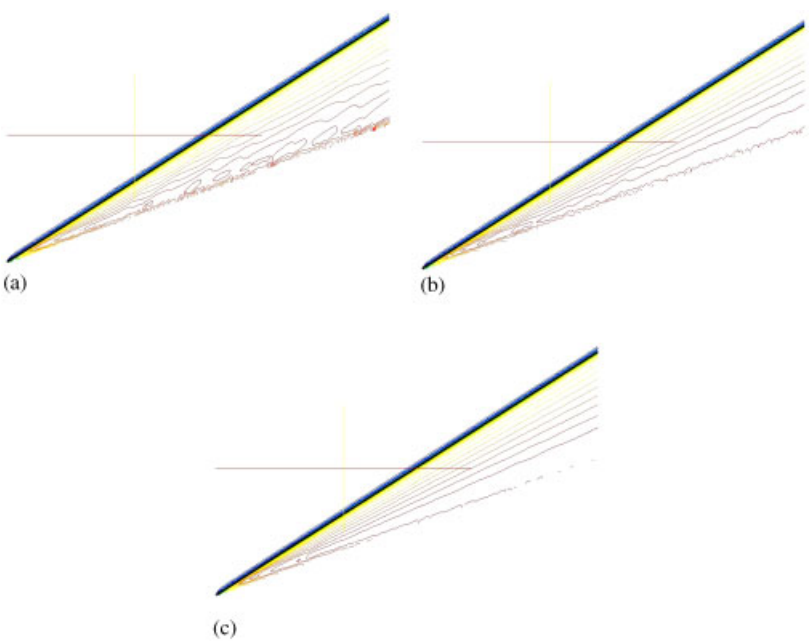

Figure 3. Density contours: (a) cone (32 subcells); (b) cone (64 subcells); and (c) cone (128 subcells).

DOI: 10.1002/fld

Note that when 32 subcells are used (Figure 3(a)) it can be observed that the surface roughness arising from a non-exact surface representation gives rise to oscillations, or 'noise' at the surface. However, the global flowfield is not too bad with the computed shock angle aligning with the exact angle (the black line) quite well.

When the number of subcells is increased to 64, the noise is reduced for the same number of contours (Figure 3(b)). By going further and using 128 subcells (Figure 3(c)), the solution exhibits even less surface noise, giving quite smooth contours. In all these examples the calculated shock angles agree very well with the exact angles. These results seem to indicate the correctness of the current VCE axisymmetric formulation and they also give the expected trend of increased solution accuracy (or decreased solution noise) for higher subcell resolutions.

The effect of the surface noise can be quantified in terms of a relative error if one compares the maximum deviation (along the cone surface) of density or pressure values from the theoretical result, i.e. $\varepsilon = |q - q_{\text{theory}}|_{\max}/q_{\text{theory}}$. However, the portion of the cone surface near the vertex is excluded from this measurement due to the numerical 'smearing' of the shock over a few cells.

It is also interesting to see what errors arise from evaluating the integrated force (per radian) along the cone surface, since the oscillating noise on the surface may to some extent 'cancel' the errors occurring from too high or too low pressure values. These errors are plotted in Figure 4 *versus* $1/N$ where N is the number of subcells. Curve fits for the pressure and density errors have also been attempted based on the equation $A + Bx^p$, with $x = 1/N$ and p thus representing a 'convergence order' for subcell resolutions based on the error.

It can be seen that the errors for the pressure and density values do decrease for higher subcell resolutions, although it appears that the solution error will not decrease to zero as subcell resolution increases. Obviously, the error also depends on the actual mesh resolution (as is the fact that for the same resolution a body-fitted grid would undoubtedly produce a more accurate

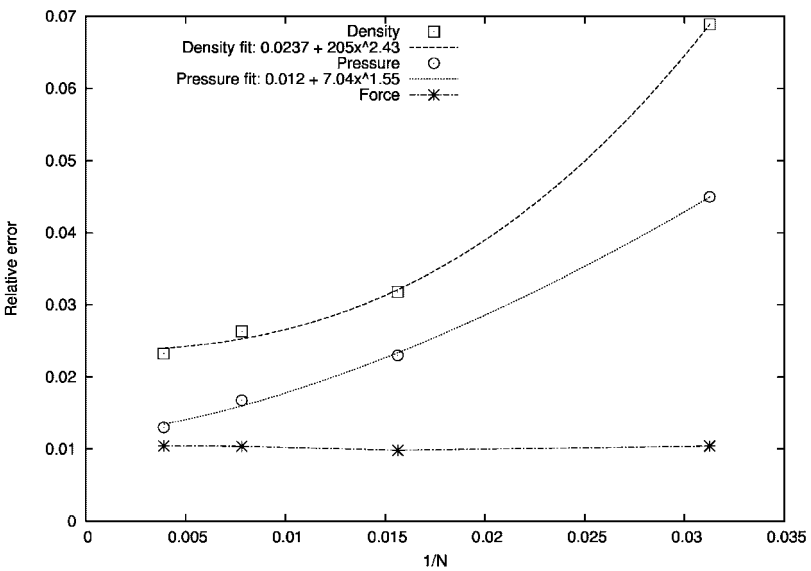

Figure 4. Noise errors.

DOI: 10.1002/fld

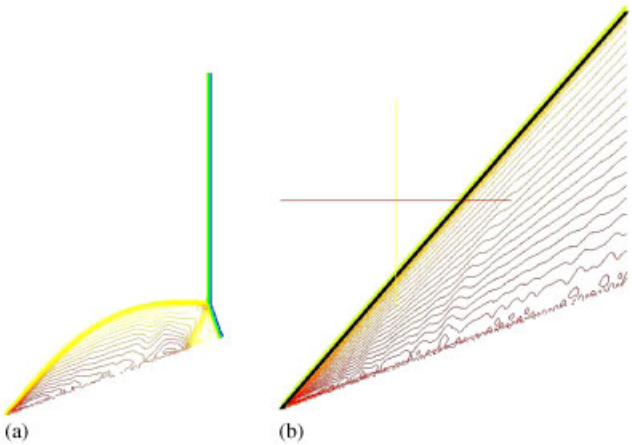

Figure 5. Density contours.

solution). The convergence orders for the pressure and density errors are 1.55 and 2.43, respectively, which is encouraging given that the underlying flow solver also has greater than first-order accuracy.

It is interesting that the integrated force error stays roughly constant with subcell resolution. This demonstrates that despite greater noise at lower resolutions, some cancellation between positive and negative amplitudes does in fact occur, leaving quite a small error at about 1% (which is probably expected with this mesh resolution and cartesian method).

3.2. Unsteady conical flow

The transient flow of a Mach 3.66 shock (with post-shock $M_\infty = 1.5$) over the cone is simulated. The number of area and side length subcells used is 64. Figure 5(a) shows the density contours before the shock has exited the domain. Some surface noise is present, but nonetheless the reflected shock, Mach stem and contact discontinuity are captured quite well. In the steady-state limit (Figure 5(b)) the result resembles the solutions in Figure 3(a). Apart from the surface noise, the general solution is not too bad with the computed shock angle again agreeing very well with the theoretical result (the black line).

4. CONCLUSION

This paper has presented an extension to the VCE method to handle axisymmetric flows. It only uses information already obtainable from the underlying VCE methodology, and thus has an accuracy consistent with and limited by the basic VCE paradigm. The produced solutions were generally good, although the expected surface noise from the approximated VCE surface representation was observed. However, this axisymmetric VCE extension (and the VCE method in general) can still give quite satisfactory results when very high-resolution solutions are not required, e.g. for practical engineering design purposes (say where one only needs integrated pressure forces).

DOI: 10.1002/fld

REFERENCES

1. Landsberg AM, Boris JP, Young TR, Scott RJ. Computing complex shocked flows through the Euler equations. *Shock Waves at Marseille*: *Proceedings of the 19th International Symposium on Shock Waves*, Marseille, France, 1993; 421–426.
2. Landsberg AM, Boris JP. The virtual cell embedding method: a simple approach for gridding complex geometries. *AIAA-97-1982*, 1997.
3. Taylor GI, Maccoll JW. The air pressure on a cone moving at high speed I. *Proceedings of the Royal Society of London*, *Series A*, 1933; **139**:278–311.
4. Van Leer B. Towards the ultimate conservative difference scheme. V. A second order sequel to Godonov's method. *Journal of Computational Physics* 1979; **32**:101–136.
5. Barth TJ, Jespersen D. The design and application of upwind schemes on unstructured meshes. *AIAA 89-0366*, 1989.
6. Wada Y, Liou MS. A flux splitting scheme with high-resolution and robustness for discontinuities. *AIAA 94-0083*, 1994.

DOI: 10.1002/fld